High Breakdown Voltage in RF AlN/GaN/AlN Quantum Well HEMTs

Austin Hickman, Reet Chaudhuri, Samuel James Bader, Kazuki Nomoto, *Member, IEEE*, Kevin Lee, Huili Grace Xing, *Senior Member, IEEE*, and Debdeep Jena, *Senior Member, IEEE*

***Abstract*—In evaluating GaN high-electron mobility transistors (HEMTs) for high-power applications, it is crucial to consider the device-level breakdown characteristics. This letter replaces the conventional AlGaN barrier and common AlGaN backbarrier with unstrained AlN, and it assesses the breakdown voltage of AlN/GaN/AlN quantum well HEMTs for gate-drain spacings in the range of 0.27–5.1 μm. The results are highlighted by a high breakdown voltage of 78 V for a gate-drain spacing of 390 nm, among the best reported for submicron-channel devices. In addition, small-signal RF measurements showed record performance for HEMTs on the AlN platform, with $f_t/f_{max} = 161/70$ GHz. The cut-off frequency and corresponding drain bias are benchmarked against the state-of-the-art GaN HEMTs using the Johnson figure of merit, with measured devices highlighted by a JFoM value of 2.2 THz · V. These results illustrate the potential for AlN/GaN/AlN quantum well HEMTs as a future platform for high-power RF transistors.**

***Index Terms*—GaN, AlN, electric breakdown, RF, power.**

I. Introduction

GALLIUM nitride-based devices have emerged as the leading contender for the future of high-voltage and high-frequency electronics. GaN's wide bandgap, large critical fields, high electron mobility, and excellent thermal conductivity enable low on-resistance and high breakdown voltages in GaN high-electron mobility transistors (HEMTs). Owing to the superior electron mobility in 2D electron gas channels, GaN HEMTs can switch high voltages at speeds unachievable by other semiconductors [1]. The electron barrier of conventional HEMTs is AlGaN on a GaN buffer. The barrier and buffer limit the carrier confinement in high-voltage applications, and moving to alloy AlGaN buffers for a back barrier in high speed applications [2]–[4] introduces a low thermal conductivity layer adversely affecting the heat dissipation.

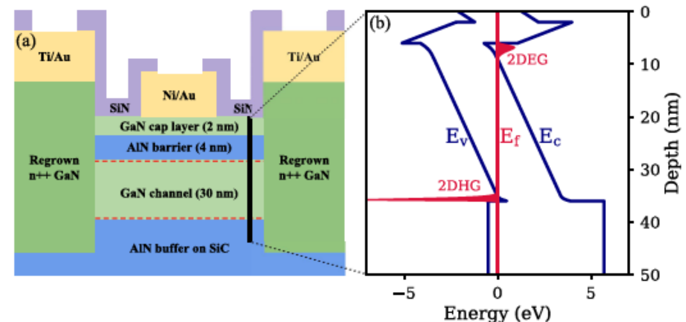

Fig. 1. (a) Cross-sectional representation of a processed QW HEMT and (b) corresponding energy band diagram simulated by 1D Poisson.

To counter these bottlenecks of the current AlGaN/GaN HEMT technology, an alternative HEMT platform based on an AlN buffer was introduced [5]. This platform uses a strained GaN quantum well sandwiched between binary AlN buffer and barrier layers. The large band offset and high polarization fields of AlN with GaN provide the maximum confinement of the 2DEG, allowing for aggressive vertical and lateral scaling. The large bandgap (~6 eV) and thermal conductivity (~340 W/mK) [6] of AlN provide an unmatched combination of electrical resistivity and thermal management in the nitride semiconductor family. A consequence of the AlN buffer region is a compressively strained, pseudomorphic GaN channel, lattice matched to AlN. The result is an unstressed AlN barrier with maximized bandgap [7], a major advantage for high-voltage applications that is unique to this heterostructure. As a bonus, the AlN platform also offers the possibility of p-channel FETs towards a nitride CMOS [8], [9].

Previously, we demonstrated the successful growth and fabrication of strained AlN/GaN/AlN quantum well HEMTs (QW HEMTs) [5], [10], [11]. The devices exhibited > 2 A/mm drain current, and potential for high-frequency performance, with an f_t/f_{max} of 124/20 GHz [11]. High-voltage properties have been previously examined for HEMTs with an AlGaN barrier [12]–[14], InAlN barrier [15]–[18], InAlGaN barrier [19], [20], AlGaN backbarrier [2], [3], [21]–[23], InGaN backbarrier [24], and N-polar HEMTs [25]–[30]. In this letter, we demonstrate the first studies of the off-state breakdown voltage for QW HEMTs, and we benchmark their breakdown voltage and on-resistance against the existing GaN HEMT platform.

Manuscript received April 28, 2019; revised June 2, 2019; accepted June 11, 2019. Date of publication June 14, 2019; date of current version July 24, 2019. This work was supported in part by the Semiconductor Research Corporation (SRC) Joint University Microelectronics Program (JUMP), Air Force Office of Scientific Research (AFOSR) under Grant FA9550-17-1-0048, NSF under Grant DMR-1710298, and this work was performed in part at the user facilities supported by NSF MRI-1338010, NSF ECCS-1542081 (Cornell NanoScale Facility), and NSF DMR-1719875 (Cornell Center for Material Research). The review of this letter was arranged by Editor Y. Wu. *(Corresponding author: Austin Hickman.)*

A. Hickman, R. Chaudhuri, K. Nomoto, and K. Lee are with the School of Electrical and Computer Engineering, Cornell University, Ithaca, NY 14853 USA (e-mail: alh288@cornell.edu).

S. J. Bader is with the School of Applied and Engineering Physics, Cornell University, Ithaca, NY 14853 USA.

H. G. Xing and D. Jena are with the School of Electrical and Computer Engineering, Department of Material Science and Engineering, Kavli Institute, Cornell University, Ithaca, NY 14853 USA.

Color versions of one or more of the figures in this letter are available online at http://ieeexplore.ieee.org.

Digital Object Identifier 10.1109/LED.2019.2923085

0741-3106 © 2019 IEEE. Personal use is permitted, but republication/redistribution requires IEEE permission.
See http://www.ieee.org/publications_standards/publications/rights/index.html for more information.

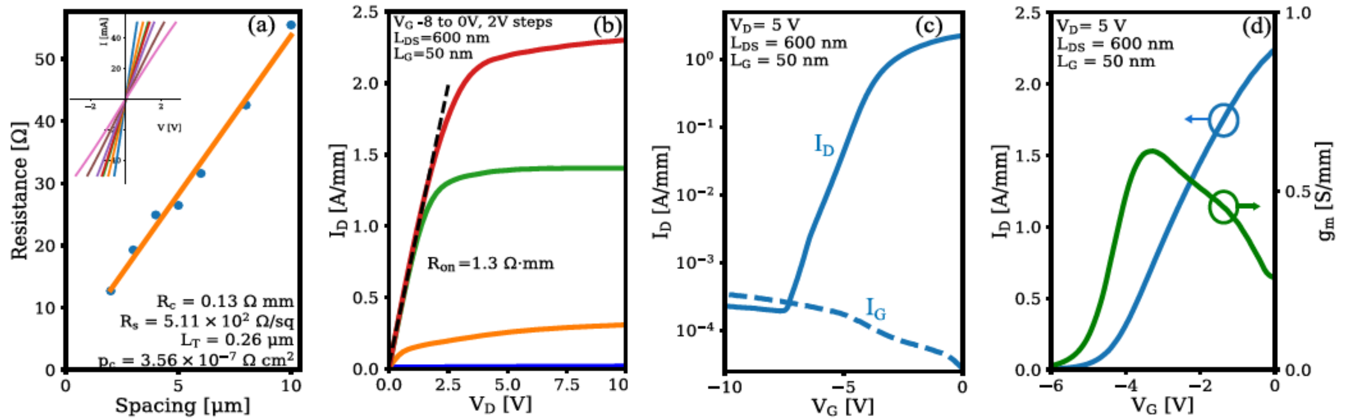

Fig. 2. (a) Linear TLM analysis of the non-annealed Ti/Au ohmic contacts to the regrown GaN. (b) I_DV_D curves demonstrating current saturation for $I_D \sim 2.3$ A/mm with low $R_{on} = 1.3\ \Omega\cdot$mm. (c) Log-scale transfer curves showing on/off ratio of 10^4 limited by gate leakage current. (d) Linear transfer curves reveal peak $g_m = 0.6$ S/mm, the highest transconductance reported for QW HEMTs.

II. Device Fabrication

The AlN/GaN/AlN epitaxial structures were grown by plasma-assisted molecular beam epitaxy (MBE) on semi-insulating 6H silicon carbide substrates. The heterostructure consists of a 350 nm AlN buffer layer, a 30 nm GaN channel, a 4 nm AlN barrier, and a 2 nm GaN passivation layer as shown in Fig. 1(a). Room temperature Hall-effect measurements prior to device fabrication showed a two-dimensional electron gas (2DEG) sheet concentration of $2.9 \cdot 10^{13}$ cm^{-2} and electron mobility of 630 cm^2/V·s, corresponding to a sheet resistance of 340 Ω/sq. The highest mobilities reported for the AlN/GaN/AlN heterostructure are currently ~700 cm^2/V · s at room temperature [5], [10], [11], [31]. Several factors may be playing a role in the mobility limitation, including the high electron concentration that may increase the electron effective mass, increased interface roughness scattering, and the possibility for a 2D hole gas (2DHG) at the GaN channel/AlN buffer interface. However, a full analysis of the mobility in this heterostructure is outside the scope of this report.

An energy band diagram of the as-grown heterostructure simulated via self-consistent solution of the Poisson and Schrodinger equations [32] shown in Fig. 1(b) shows the formation of a 2DEG at the top AlN/GaN heterojunction. The simulation also indicates the formation of a 2DHG at the bottom GaN/AlN heterojunction. The 2DHG has been experimentally detected in the AlN/GaN/AlN heterostructure via terahertz spectroscopy [33], and it has been confirmed in an undoped GaN/AlN heterostructure [34]. If present in the QW HEMT, the 2DHG may act as a floating body or dynamic field plate, depending on the contact quality. The behavior of the 2DHG merits more detailed studies in the future.

The device fabrication used a realigned gate-last process. The heterostructure was patterned with a SiO_2/chromium hard mask and etched via BCl_3 inductively coupled plasma (ICP) to expose the 2DEG sidewall. The sample was loaded back into the MBE, and regrown n++ GaN ($N_D \sim 10^{20}$cm^{-3}) source/drain contacts were formed. The SiO_2/Cr mask was removed via HF, and device isolation was achieved by another BCl_3 ICP etch that extended 20 nm into the AlN buffer. Ti/Au (50/50 nm) non-alloyed ohmic contacts were deposited by e-beam evaporation on top of the regrown GaN source/drain regions. Long-channel gates were patterned by photolithography, and Ni/Au (50/50 nm) Schottky contacts were deposited by e-beam evaporation directly on the sample surface. Submicron channel devices were patterned for RF gates using electron beam lithography (EBL) with a PMMA bilayer. Ni/Au (20/50 nm) Schottky contacts were deposited via e-beam evaporation directly on the sample surface. Gate lengths as short as 40 nm were observed via SEM, shown in Fig. 4(a). No field plate was implemented. The HEMTs were then passivated with low-power, plasma-enhanced chemical vapor deposition (PECVD) silicon nitride with a thickness of 40 nm. Contact holes were formed in the silicon nitride by 6:1 BOE etching to allow probing of the ohmic and gate contact pads. The final HEMT cross-section is shown in Fig. 1(a).

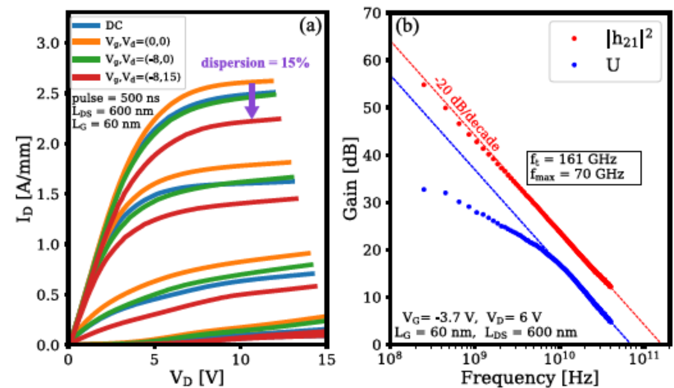

Fig. 3. (a) Pulsed $I_D - V_{DS}$ measurements after SiN passivation of a QW HEMT with $L_G = 60$ nm, demonstrating moderate dispersion up to 15 V. (b) Small-signal measurements of the passivated QW HEMT with $f_t/f_{max} = 161/70$ GHz.

III. Experimental Results and Discussion

After device fabrication, transfer-length method (TLM) patterns were measured in multiple locations across the sample, revealing excellent ohmic contact to the 2DEG with a contact resistance of $R_c = 0.13\ \Omega\cdot$mm, shown in Fig. 2(a). Hall-effect measurements at room temperature after fabrication revealed a 2DEG sheet concentration of $3 \cdot 10^{13}$ cm^{-2} and an electron mobility of 410 cm^2/V · s, resulting in a sheet resistance of

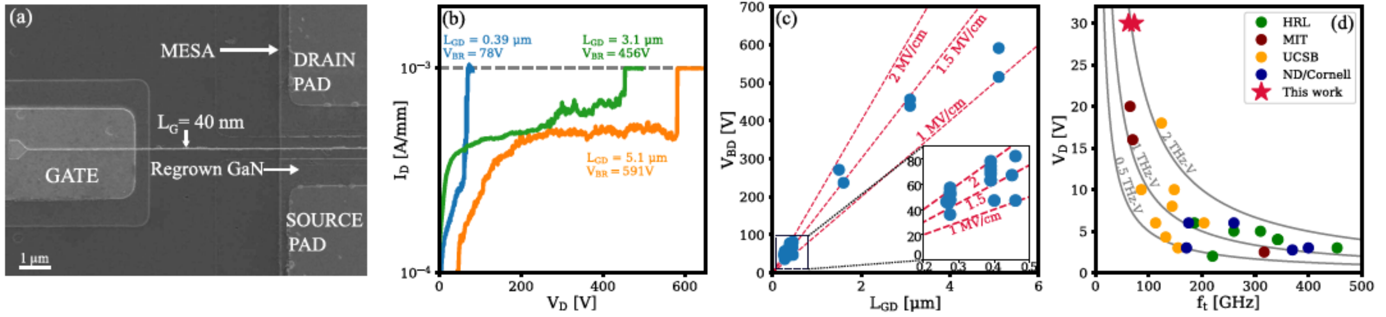

Fig. 4. (a) SEM image of a short-channel QW HEMT with $L_G = 40$ nm. (b) Hard breakdown for three HEMTs with varied gate-drain separations. (c) Breakdown voltage scaling as a function of gate-drain separation ranging from 0.27 to 5.1 μm. (d) Johnson figure of merit benchmark plot comparing the QW HEMT to state-of-the-art GaN HEMTs with submicron L_{GD} and no field plate.

510 Ω/sq. The sheet resistance increased 50% from its as-grown value, likely due to surface damage induced during the fabrication process and could be potentially avoided by changing the SiO_2 deposition process. Transfer I-V characteristics reveal an $I_{on}/I_{off} = 10^4$ (this value was 10^9 before passivation) with a peak transconductance of 0.6 S/mm, as shown in Fig. 2(c, d). This is the highest transconductance reported for devices on the AlN/GaN/AlN heterostructure platform and shows their high promise. The output characteristics, plotted in Fig. 2(b), show a drain current of ~2.3 A/mm with excellent saturation and on-resistance of 1.3 Ω·mm.

Pulsed $I_D - V_{DS}$ measurements were performed after silicon nitride passivation to verify dispersion control, shown for a QW HEMT with $L_G = 60$ nm in Fig. 3(a). Bias-dependent S-parameters were then measured in the range of 0.05-40 GHz. The system was de-embedded via a short-open-load-through (SOLT) impedance standard substrate and on-wafer open/short structures. The f_t and f_{max} values were extracted from $|h_{21}|^2$ and unilateral (U) gain plots. The device measured for dispersion also demonstrated $f_t = 161$ GHz, $f_{max} = 70$ GHz, as shown in Fig. 3(b). Both f_t and f_{max} values are records for HEMTs on the AlN platform. Further scaling of gate length and incorporation of a T-gate geometry are expected to dramatically increase f_t and f_{max} for the QW HEMT.

To investigate breakdown characteristics, the gate voltage was set below the threshold voltage (typically $V_G = -8$ V), and V_{DS} was increased until HEMT breakdown occurred. The breakdown voltage metric is defined as $I_D \geq 1$ mA/mm. QW HEMTs were tested for gate-drain lengths (L_{GD}) ranging from 270 nm to 5.1 μm. The devices were covered in Fluorinert during the measurement process.

Fig. 4(b) shows the three terminal off-state breakdown of three QW HEMTs with varied gate-drain distances. Among all devices, the highest breakdown voltage observed is $V_{BD} = 591$ V ($L_{GD} = 5.1$ μm), corresponding to an average electric field (E_{BD}) of 1.16 MV/cm. All measured devices had average electric fields above 1 MV/cm at breakdown. During the measurement process and prior to breakdown, the gate current is found to be roughly equal to the drain current. This indicates the off-state drain current and breakdown is dominated by gate-drain leakage and not avalanche or channel breakdown, and is far from the material limits. Future breakdown measurements may improve by refining the SiN passivation process to minimize any increase in the gate leakage current.

To explore the potential for high-frequency applications, submicron channel lengths were examined for breakdown. A breakdown voltage of 78 V was measured for a HEMT with 390 nm gate-drain distance. This corresponds to an effective breakdown field of 2 MV/cm. This is among the largest breakdown voltages reported for a submicron channel nitride HEMT, demonstrating the potential of QW HEMTs for extremely high-power operation in RF applications. Fig. 4(c) shows the scaling of breakdown voltage as a function of L_{GD}. The breakdown voltage does not scale linearly with L_{GD}, which is expected due to the non-uniform distribution of the E-field within the channel.

IV. Conclusions and Benchmarking

Small-signal s-parameters were also measured for two QW HEMTs with $L_G = 80$ nm, $L_{GD} = 460$ μm at high drain biases to demonstrate simultaneous high-voltage, high-frequency performance. For a drain bias of 30 V, the devices showed cutoff frequencies of 73 and 62 GHz. The measured cutoff frequency and corresponding drain bias were benchmarked against state-of-the-art GaN HEMTs with submicron L_{GD} and no field plate [2], [3], [12]–[23], [25]–[30] using the Johnson figure of merit (JFoM), as shown in Fig. 4(d). The two devices measured at high drain bias yielded JFoM values of 2.2 and 1.9 THz·V, among the highest reported. Large-signal power performance is to be verified in future work.

In this letter, the breakdown characteristics of strained AlN/GaN/AlN quantum well HEMTs were explored for the first time. The fabricated devices demonstrated excellent DC characteristics, with $R_c = 0.13$ Ω·mm, $I_{Dsat} = 2.3$ A/mm, and peak $g_m = 0.6$ S/mm. HEMTs with L_{GD} ranging from 270 nm to 5.1 μm were tested for breakdown characteristics, and a clear dependence of breakdown voltage on gate-drain distance is observed. Small-signal RF measurements revealed record performance for HEMTs on the AlN platform, with $f_t/f_{max} = 161/70$ GHz. High breakdown voltage is observed across all gate-drain lengths, most notably for submicron channel devices, in which a breakdown voltage of 78 V was measured for a device with $L_{GD} = 390$ nm, $L_{SD} = 800$ nm. The combination of high breakdown voltage and promising small-signal response demonstrate QW HEMTs as a viable platform and potential successor to AlGaN/GaN HEMTs for future high-power RF electronics.

References

[1] M. Danilovic, Z. Chen, R. Wang, F. Luo, D. Boroyevich, and P. Mattavelli, "Evaluation of the switching characteristics of a gallium-nitride transistor," in *Proc. IEEE Energy Convers. Congr. Expo. (ECCE)*, Sep. 2011, pp. 2681–2688.

[2] K. Shinohara, A. Corrion, D. Regan, I. Milosavljevic, D. Brown, S. Burnham, P. J. Willadsen, C. Butler, A. Schmitz, D. Wheeler, A. Fung, and M. Micovic, "220GHz fTand 400GHz fmaxin 40-nm GaN DH-HEMTs with re-grown ohmic," in *IEDM Tech. Dig.*, Dec. 2010, pp. 30.1.1–30.1.4.

[3] K. Shinohara, D. Regan, I. Milosavljevic, A. L. Corrion, D. F. Brown, P. J. Willadsen, C. Butler, A. Schmitz, S. Kim, V. Lee, A. Ohoka, P. M. Asbeck, and M. Micovic, "Electron velocity enhancement in laterally scaled GaN DH-HEMTs With f_T of 260 GHz," *IEEE Electron Device Lett.*, vol. 32, no. 8, pp. 1074–1076, Aug. 2011.

[4] D. S. Lee, X. Gao, S. Guo, and T. Palacios, "InAlN/GaN HEMTs with AlGaN back barriers," *IEEE Electron Device Lett.*, vol. 32, no. 5, pp. 617–619, May 2011. [Online]. Available: http://ieeexplore.ieee.org/document/5723687/

[5] G. Li, R. Wang, J. Guo, J. Verma, Z. Hu, Y. Yue, F. Faria, Y. Cao, M. Kelly, T. Kosel, H. G. Xing, and D. Jena, "Ultrathin body GaN-on-insulator quantum well FETs with regrown ohmic contacts," *IEEE Electron Device Lett.*, vol. 33, no. 5, pp. 661–663, May 2012.

[6] R. Rounds, B. Sarkar, A. Klump, C. Hartmann, T. Nagashima, R. Kirste, A. Franke, M. Bickermann, Y. Kumagai, Z. Sitar, and R. Collazo, "Thermal conductivity of single-crystalline AlN," *Appl. Phys. Express*, vol. 11, no. 7, 2018, Art. no. 071001.

[7] G. Li, B. Song, S. Ganguly, M. Zhu, R. Wang, X. Yan, J. Verma, V. Protasenko, H. G. Xing, and D. Jena, "Two-dimensional electron gases in strained quantum wells for AlN/GaN/AlN double heterostructure field-effect transistors on AlN," *Appl. Phys. Lett.*, vol. 104, no. 19, 2014, Art. no. 193506.

[8] G. Li, R. Wang, B. Song, J. Verma, Y. Cao, S. Ganguly, A. Verma, J. Guo, H. G. Xing, and D. Jena, "Polarization-induced GaN-on-insulator E/D Mode p-channel heterostructure FETs," *IEEE Electron Device Lett.*, vol. 34, no. 7, pp. 852–854, Jul. 2013.

[9] S. J. Bader, R. Chaudhuri, K. Nomoto, A. Hickman, Z. Chen, H. W. Then, D. A. Muller, H. G. Xing, and D. Jena, "Gate-recessed E-mode p-channel HFET with high on-current based on GaN/AlN 2D hole gas," *IEEE Electron Device Lett.*, vol. 39, no. 12, pp. 1848–1851, Dec. 2018.

[10] S. M. Islam, M. Qi, B. Song, K. Nomoto, V. Protasenko, J. Wang, S. Rouvimov, P. Fay, H. G. Xing, and D. Jena, "First demonstration of strained AlN/GaN/AlN quantum well FETs on SiC," in *Proc. 74th Annu. Device Res. Conf.*, no. 10, Jun. 2016, pp. 1–2.

[11] M. Qi, G. Li, S. Ganguly, P. Zhao, X. Yan, J. Verma, B. Song, M. Zhu, K. Nomoto, H. Xing, and D. Jena, "Strained GaN quantum-well FETs on single crystal bulk AlN substrates," *Appl. Phys. Lett.*, vol. 110, no. 6, Feb. 2017, Art. no. 063501.

[12] T. Palacios, C. S. Suh, A. Chakraborty, S. Keller, S. P. DenBaars, and U. K. Mishra, "High-performance E-mode AlGaN/GaN HEMTs," *IEEE Electron Device Lett.*, vol. 27, no. 6, pp. 428–430, Jun. 2006.

[13] T. Palacios, E. Snow, Y. Pei, A. Chakraborty, S. Keller, S. P. DenBaars, and U. K. Mishra, "Ge-spacer technology in AlGaN/GaN HEMTs for mm-wave applications," in *IEDM Tech. Dig.*, vol. 1, no. 805, Dec. 2005, pp. 787–789.

[14] J. W. Chung, W. E. Hoke, E. M. Chumbes, and T. Palacios, "AlGaN/GaN HEMT With 300-GHz f_{max}," *IEEE Electron Device Lett.*, vol. 31, no. 3, pp. 195–197, Mar. 2010.

[15] J. W. Chung, O. I. Saadat, J. M. Tirado, X. Gao, S. Guo, and T. Palacios, "Gate-recessed InAlN/GaN HEMTs on SiC substrate with Al_2O_3 passivation," *IEEE Electron Device Lett.*, vol. 30, no. 9, pp. 904–906, Sep. 2009.

[16] B. Sensale-Rodriguez, J. Guo, R. Wang, J. Verma, G. Li, T. Fang, E. Beam, A. Ketterson, M. Schuette, P. Saunier, X. Gao, S. Guo, G. Snider, P. Fay, D. Jena, and H. G. Xing, "Time delay analysis in high speed gate-recessed E-mode InAlN HEMTs," *Solid-State Electron.*, vol. 80, pp. 67–71, Feb. 2013. doi: 10.1016/j.sse.2012.10.004.

[17] Y. Yue, Z. Hu, J. Guo, B. Sensale-Rodriguez, G. Li, R. Wang, F. Faria, T. Fang, B. Song, X. Gao, S. Guo, T. Kosel, G. Snider, P. Fay, D. Jena, and H. Xing, "InAlN/AlN/GaN HEMTs with regrown ohmic contacts and f_T of 370 GHz," *IEEE Electron Device Lett.*, vol. 33, no. 7, pp. 988–990, Jul. 2012.

[18] Y. Yue, Z. Hu, J. Guo, B. Sensale-Rodriguez, G. Li, R. Wang, F. Faria, B. Song, X. Gao, S. Guo, T. Kosel, G. Snider, P. Fay, D. Jena, and H. G. Xing, "Ultrascaled InAlN/GaN high electron mobility transistors with cutoff frequency of 400 GHz," *Jpn. J. Appl. Phys.*, vol. 52, no. 8S, pp. 1–2, 2013.

[19] R. Wang, G. Li, G. Karbasian, J. Guo, F. Faria, Z. Hu, Y. Yue, J. Verma, O. Laboutin, Y. Cao, W. Johnson, G. Snider, P. Fay, D. Jena, and H. Xing, "InGaN channel high-electron-mobility transistors with InAlGaN barrier and f_T/f_{max} of 260/220 GHz," *Appl. Phys. Express*, vol. 6, no. 1, 2013, Art. no. 016503.

[20] D. S. Lee, O. Laboutin, Y. Cao, W. Johnson, E. Beam, A. Ketterson, M. Schuette, P. Saunier, D. Kopp, P. Fay, and T. Palacios, "317 GHz InAlGaN/GaN HEMTs with extremely low on-resistance," *Phys. Status Solidi C, Current Topics Solid State Phys.*, vol. 10, no. 5, pp. 827–830, May 2013.

[21] K. Shinohara, D. Regan, A. Corrion, D. Brown, S. Burnham, P. J. Willadsen, I. Alvarado-Rodriguez, M. Cunningham, C. Butler, A. Schmitz, S. Kim, B. Holden, D. Chang, V. Lee, A. Ohoka, P. M. Asbeck, and M. Micovic, "Deeply-scaled self-aligned-gate GaN DH-HEMTs with ultrahigh cutoff frequency," in *IEDM Tech. Dig.*, vol. 2, Dec. 2011, pp. 19.1.1–19.1.4.

[22] K. Shinohara, D. Regan, A. Corrion, D. Brown, Y. Tang, J. Wong, G. Candia, A. Schmitz, H. Fung, S. Kim, and M. Micovic, "Self-aligned-gate GaN-HEMTs with heavily-doped n^+-GaN ohmic contacts to 2DEG," in *IEDM Tech. Dig.*, Dec. 2012, pp. 27.2.1–27.2.4. [Online]. Available: http://ieeexplore.ieee.org/document/6479113/

[23] Y. Tang, K. Shinohara, D. Regan, A. Corrion, D. Brown, J. Wong, A. Schmitz, H. Fung, S. Kim, and M. Micovic, "Ultrahigh-speed GaN high-electron-mobility transistors with f_T/f_{max} of 454/444 GHz," *IEEE Electron Device Lett.*, vol. 36, no. 6, pp. 549–551, Jun. 2015.

[24] J. Liu, Y. Zhou, J. Zhu, K. M. Lau, and K. J. Chen, "AlGaN/GaN/InGaN/GaN DH-HEMTs with an InGaN notch for enhanced carrier confinement," *IEEE Electron Device Lett.*, vol. 27, no. 1, pp. 10–12, Jan. 2006.

[25] Nidhi, S. Dasgupta, D. F. Brown, S. Keller, J. S. Speck, and U. K. Mishra, "N-polar GaN-based highly scaled self-aligned MIS-HEMTs with state-of-the-art $f_T.L_G$ product of 16.8 GHz-μm," in *IEDM Tech. Dig.*, no. 805, Dec. 2009, pp. 1–3.

[26] Nidhi, S. Dasgupta, J. Lu, J. S. Speck, and U. K. Mishra, "Self-aligned N-polar GaN/InAlN MIS-HEMTs with record extrinsic transconductance of 1105 mS/mm," *IEEE Electron Device Lett.*, vol. 33, no. 6, pp. 794–796, Jun. 2012.

[27] D. Denninghoff, J. Lu, M. Laurent, E. Ahmadi, S. Keller, and U. K. Mishra, "N-polar GaN/InAlN MIS-HEMT with 400-GHz Æ'$_{max}$," in *Proc. 70th Device Res. Conf.*, vol. 32, no. 7, Jun. 2012, pp. 151–152.

[28] D. J. Denninghoff, S. Dasgupta, J. Lu, S. Keller, and U. K. Mishra, "Design of high-aspect-ratio T-gates on N-polar GaN/AlGaN MIS-HEMTs for high f_{max}," *IEEE Electron Device Lett.*, vol. 33, no. 6, pp. 785–787, Jun. 2012.

[29] D. Denninghoff, J. Lu, E. Ahmadi, S. Keller, and U. K. Mishra, "N-polar GaN/InAlN/AlGaN MIS-HEMTs with 1.89 S/mm extrinsic transconductance, 4 A/mm drain current, 204 GHz fTand 405 GHz f_{max}," in *Proc. 71st Device Res. Conf.*, Jun. 2013, vol. 33, no. 7, pp. 197–198.

[30] B. Romanczyk, S. Wienecke, M. Guidry, H. Li, E. Ahmadi, X. Zheng, S. Keller, and U. K. Mishra, "Demonstration of constant 8 W/mm power density at 10, 30, and 94 GHz in state-of-the-art millimeter-wave N-polar GaN MISHEMTs," *IEEE Trans. Electron Devices*, vol. 65, no. 1, pp. 45–50, Jan. 2018.

[31] S. Rennesson, M. Leroux, M. Al Khalfioui, M. Nemoz, S. Chenot, J. Massies, L. Largeau, E. Dogmus, M. Zegaoui, F. Medjdoub, and F. Semond, "Ultrathin AlN-based HEMTs grown on silicon substrate by NH_3-MBE," *Physica Status Solidi A, Appl. Mater. Sci.*, vol. 215, no. 9, 2018, Art. no. 1700640.

[32] I. H. Tan, G. L. Snider, L. D. Chang, and E. L. Hu, "A self-consistent solution of Schrödinger–Poisson equations using a nonuniform mesh," *J. Appl. Phys.*, vol. 68, no. 8, pp. 4071–4076, 1990.

[33] H. C. Quispe, S. M. Islam, S. Bader, A. Chanana, K. Lee, R. Chaudhuri, A. Nahata, H. G. Xing, D. Jena, B. Sensale-Rodriguez, "Terahertz spectroscopy of an electron-hole bilayer system in AlN/GaN/AlN quantum wells," *Appl. Phys. Lett.*, vol. 111, no. 7, 2017, Art. no. 073102.

[34] R. Chaudhuri, S. J. Bader, Z. Chen, D. A. Müller, H. Xing, and D. Jena, "A polarization-induced 2D hole gas in undoped gallium nitride quantum wells," 2018, *arXiv:1807.08836*. [Online]. Available: https://arxiv.org/abs/1807.08836